Liver 2001: 21: 1–12
Printed in Denmark . All rights reserved

Liver
ISSN 0106-9543

Involvement of reactive oxygen species and nitric oxide radicals in activation and proliferation of rat hepatic stellate cells

Svegliati-Baroni G, Saccomanno S, van Goor H, Jansen P, Benedetti A, Moshage H. Involvement of reactive oxygen species and nitric oxide radicals in activation and proliferation of rat hepatic stellate cells. Liver 2001: 21: 1–12. © Munksgaard, 2001

Abstract: *Background /Aims:* Reactive oxygen species (ROS) induce HSCs activation, proliferation and collagen gene expression *in vitro*. Nitric oxide (NO) represents a reactive molecule that reacts with ROS, yielding peroxynitrite. We thus verified the effect of NO on ROS-induced HSCs proliferation *in vitro* and correlated iNOS expression and ROS formation to HSCs activation in the early phase of liver injury leading to hepatic fibrosis *in vivo*. *Methods/Results*: HSCs were incubated with iron ascorbate (FeAsc) *in vitro*, which induced ROS production, ERK1/2 phosphorylation and increased cell proliferation. This effect was significantly reduced by the presence of the NO donor S-nitroso-N-acetylpenicillamine. Liver injury was induced *in vivo* in rats by dimethylnitrosamine administration. HSCs activation started 6 h after DMN administration and peaked at 1 week. ROS generation and neutrophil infiltration were evident for at least 48 h after DMN treatment, showing an identical distribution pattern. Only a few inflammatory cells expressed iNOS 6 h after DMN administration. *Conclusions:* we have shown that NO acts as a ROS scavenger *in vitro*, thus inhibiting HSCs proliferation. ROS production by infiltrating neutrophils occurs in the early phase of liver fibrosis and can represent a stimulus to HSCs activation *in vivo*. The reduced iNOS expression may account for the low NO levels and the inability to prevent the ROS-induced HSC activation *in vivo*.

Gianluca Svegliati-Baroni[1], Stefania Saccomanno[1], Harry van Goor[2], Peter Jansen[2], Antonio Benedetti[1] and Han Moshage[2]

[1]Department of Gastroenterology, University of Ancona, Italy and [2]Department of Gastroenterology and Hepatology, University Hospital Groningen, The Netherlands

Key words: liver injury – reactive oxygen species – nitric oxide – hepatic stellate cells

Dr. Gianluca Svegliati-Baroni, M.D., Clinica di Gastroenterologia, Facoltà di Medicina, Nuovo Polo Didattico, III Piano, Ospedale Regionale Torrette, 60020 Ancona, Italy.
Tel: +39 71 2206043. Fax: +39 71 2206044.
e-mail: gsvegliati@unian.it

Received 28 February, accepted 1 August 2000

Hepatic fibrosis represents a common response to chronic liver injury, independently from the etiologic agent (virus, ethanol, metabolic diseases). Activation of hepatic stellate cells (HSCs) is a key feature of liver fibrosis (1). Activated HSCs display an increased expression of matrix genes and α-smooth muscle actin (αSMA) as well as increased proliferation. The process of HSCs activation can be studied using different experimental models of liver fibrosis (2) in which perisinusoidal αSMA-positive cells proliferate, accumulate close to necrotic areas from which fibrotic septa will develop later on, and produce excessive amounts of extracellular matrix proteins (3–6). Several *in vitro* and *in vivo* data have suggested that formation of reactive oxygen species (ROS) could represent a common link between the different forms of chronic liver injury and hepatic fibrosis (7). Formation of reactive oxygen species has been reported *in vivo* in several models of liver fibrosis (2, 6–8) while, *in vitro*, reactive oxygen species have been shown to stimulate HSCs activation, proliferation and collagen synthesis by acting as intracellular signaling molecules (9–12). Despite these reports, only a few experimental data linking the earliest phase of liver fibrosis to formation of reactive oxygen species and HSCs activation have been reported (13).

Nitric oxide (NO) is a biologically active radical synthesized by the enzyme nitric oxide synthase (NOS). Three isoforms of this enzyme exist, all requiring L-arginine and oxygen. Neuronal (type I, nNOS) NOS and endothelial (type III, eNOS) NOS are Ca^{2+}- and calmodulin-dependent constitutive isoforms (14–16). These constitutive iso-

forms have important functions under normal conditions. The constitutive isoforms are rapidly activated by intracellular Ca^{2+} fluxes and produce small quantities of $NO^{\cdot}$ (14–16). Inducible NOS (iNOS, type II) is not expressed under normal conditions; it is induced by cytokines and/or endotoxin during inflammatory and infectious processes and produces large amounts of $NO^{\cdot}$ for extended periods of time (14–16). NO is able to react with reactive oxygen species (ROS), yielding peroxynitrite. This reaction eliminates ROS and could therefore be favorable. On the other hand, peroxynitrite is a very reactive, toxic and strongly oxidizing compound. Whether the formation of peroxynitrite is detrimental or beneficial will depend on the exact conditions of the local microenvironment (e.g. the relative amounts of NO and ROS formed, the presence of antioxidants and ROS scavenging enzyme systems like SOD, and pH) (17, 18). Therefore, we tested whether NO, as a scavenger of ROS, affects the activation and/or proliferation of HSCs, using the following strategies:

- the effect of NO donors on ROS-induced HSCs proliferation *in vitro* was investigated;
- the expression of iNOS and formation of ROS was investigated during the activation process of HSCs using the dimethylnitrosamine model of liver fibrosis (3, 5).

Materials

Culture media were from GIBCO (Grand Island, NY). Nycodenz was from Life Technologies (Milan, Italy). Bromodeoxyuridine and diaminobenzidine were from Fluka (Flukachemie AG, Buchs, Switzerland). Nitrocellulose membranes (Hybond) were from Amersham (Milan, Italy). Pronase was from Boehringer Mannheim (Monza, Italy). Monoclonal anti-bromodeoxyuridine and peroxidase-conjugated rabbit anti-mouse immunoglobulins were from Dako (Glostrup, Denmark). All other reagents were from Sigma Chemical Co., Milan, Italy.

Methods

In vitro study

HSCs isolation and culture

HSCs were isolated from male Sprague-Dawley rats (300–500 g) after collagenase-pronase perfusion of the liver followed by Nycodenz gradient (12% w/v) centrifugation as described previously (10, 11, 19).

Cells were then cultured in Iscove Modified Dulbecco's Medium (IMDM) supplemented with 20% fetal bovine serum, 2 mmol/l glutamine, and 1% antibiotic-antifungal solution at 37°C in a humidified atmosphere containing 5% CO_2. The medium was replaced 24 h after seeding and every 48 h thereafter.

Primary cultures of HSCs were allowed to grow to confluence, subcultured by trypsinization (0.025% trypsin/0.5 mmol/l ethylenediaminetetraacetic acid) and then cultured in the same medium as above. Experiments described in this study were performed in triplicate on cells between the first and third serial passages using three independent cell lines.

Determination of HSCs proliferation

HSCs proliferation was measured by indirect immunoperoxidase staining of nuclei which had incorporated bromodeoxyuridine (BrdU) (9–11, 19). Briefly, 72 h after trypsinization, HSCs were incubated in IMDM containing 0.5% FBS for 24 h. Thereafter, the medium was removed and cells were incubated in the same medium containing test substances for an additional 24 h. BrdU was added (5×10^{-5} M) during the last 4 h of incubation. At the end of the incubation period, cell monolayers were washed twice with ice-cold Tris-buffer saline (TBS) (pH 7.6) and then fixed with 80% acetone. DNA was denatured by incubating cells for 45 min at 70°C with 95% formamide (vol/vol) dissolved in sodium citrate (0.15 mol/l). Thereafter, cells were incubated for 2 h at room temperature with anti-BrdU immunoglobulins (1:50 in TBS/bovine serum albumin (BSA) 1%). After washing two times with TBS/BSA, cells were incubated with peroxidase-conjugated rabbit anti-mouse immunoglobulins (1:50 in TBS/BSA containing 5% rat serum) for 30 min at room temperature. Nuclei that had taken up BrdU were stained using diaminobenzidine as substrate and counted using a computerized image analysis system connected to an Olympus microscope (Olympus Vanox AHBT3, Olympus Optical Co. Ltd., Tokyo, Japan). Data were expressed as % of BrdU positive nuclei.

NO and ROS donors and antioxidants

S-nitroso-N-acetylpenicillamine (SNAP) was used as NO donor and added at a final concentration of 1 mmol/l to culture medium. Incubation of 1 mmol/l SNAP in culture medium without cells resulted in a gradual increase in NO concentration (15–20 μmol NO/l per hour), resulting in a NO concentration of 400–600 μmol NO/l after 24 h. NO accumulation is taken as a reliable reflection of NO generation. Production of ROS (superoxide anion) in culture medium containing 50 μmol/l Fe^{2+} per 100 μmol/l ascorbate (FeAsc) (12) was confirmed using the cytochrome c assay in the absence of cells (20). Some experiments were also

performed in the presence of superoxide dismutase (SOD, 300 U/ml) and catalase (500 U/ml) as ROS scavengers. The effectivity of ROS scavengers was confirmed using the cytochrome c assay in culture medium in the absence of cells (20).

70 kD S6 kinase and ERK activation

Data from the literature indicate that different intracellular pathways that involve either the phosphatidylinositol 3-kinase (PI3-K) or the extracellular-signal regulated kinase (ERK1/2) play a key role in regulating HSC proliferation (21, 22). To evaluate the effect of FeAsc on these pathways in HSC, cells were incubated in IMDM containing 0.5% FBS for 24 h. Thereafter, the medium was removed and cells were incubated in the same medium containing FeAsc for additional 15 and 30 min. In parallel experiments, cells were also exposed to 1 mmol/l SNAP for 30 min before FeAsc incubation.

Cell were then scraped and homogenized in ice cold buffer (pH 7.4) consisting of 50 mmol/l Tris, 150 mmol/l KCl, 1% Triton X-100, 1 mmol/l ethylenediaminetetraacetic acid, 5 mmol/l N-ethylmaleimide, 0.2 mmol/l phenylmethylsulfonylfluoride. The Western blot technique was then performed using specific antibodies against 70 kD S6 kinase and tyrosine-phosphorylated ERK1/2 as previously described (21).

In vivo study

Experimental design

Thirty male Sprague-Dawley rats were used. They were fed a pellet diet (Nossan, Italy) according to good laboratory practice. Rats were housed in plastic cages with a wire-mesh base providing isolation from a hygienic bed and were exposed to a 12-h, controlled light cycle. Experiments were performed in accordance with the institutional ethical guidelines.

Hepatic injury was induced by intraperitoneal injections of 10 mg/kg of DMN dissolved in saline to obtain a 1% solution (3, 5). DMN was administered for 3 consecutive days. To study the early events leading to liver fibrosis, animals were killed 6, 24, 48 h and 1 week after the third DMN injection. Control animals received saline.

Preparation of tissue

Liver specimens were routinely fixed in 4% phosphate-buffered formaldehyde or in methanol for 18–24 h and embedded in paraffin. Tissue sections (4 μm thick) were stained with hematoxylin-eosin for routine examination or with Sirius Red for collagen visualization.

Other specimens were embedded in OCT compound (Triangle Biomedical Sciences, Durham, NC), immediately snap-frozen in isopentane (precooled in liquid nitrogen) and then stored at −80 °C until used.

For Western blotting, the remaining liver was cut into 150-mg pieces, dipped in liquid nitrogen and then stored at −80 °C until used.

Immunohistochemistry

Identification of proliferating and activated HSCs

For the simultaneous detection of alpha smooth muscle actin (αSMA), as a marker of activated HSCs (1, 3, 5), and PCNA, as a marker of S-phase cells (23), a sequential double immunoenzymatic reaction was performed using methanol fixed sections as previously described (3, 5).

In the first sequence, visualization of αSMA-positive cells was obtained by a three-step immunoperoxidase technique. Liver sections were sequentially incubated with mouse monoclonal antibody against αSMA (Sigma A2547, 1:50 dilution), peroxidase-conjugated rabbit anti-mouse immunoglobulins (Dako P161, 1:50 dilution) and peroxidase-conjugated swine anti-rabbit immunoglobulins (Dako P217, 1:50 dilution). The reaction, which resulted in a brown staining of cytoplasmic reactive sites, was visualized by incubation in Tris-buffered saline containing 0.06% diaminobenzidine (DAB) and 0.01% H_2O_2.

In the second sequence, liver sections were incubated with mouse monoclonal antibody against PCNA (Dako M879, 1:100 dilution) followed by peroxidase-conjugated rabbit anti-mouse immunoglobulins. S-phase nuclei were finally visualized by a magenta color after incubation with the peroxidase substrate 3-amino-9-ethylcarbazole (AEC, 0.5% in 0.05 M acetate buffer).

Neutrophils and iNOS identification

The rabbit polyclonal antibody against rat iNOS and the His48 monoclonal antibody, which specifically recognizes rat neutrophils, were developed in our laboratory and have been described before (24, 25).

For immunohistochemistry, 4-μm cryostat sections were cut. After air-drying, sections were fixed in acetone for 10 min at room temperature and air-dried again. Subsequently, they were washed in PBS (pH 7.4) and incubated in the rat polyclonal iNOS antibody (1:300 in PBS containing 1% BSA) or in undiluted His48 hybridoma supernatant for 60 min at room temperature. After incubation with the first antibody, endogenous peroxidase activity was blocked by incubating for 30 min in PBS containing 0.075% H_2O_2. For iNOS, secondary antibodies were peroxidase-conjugated goat anti-rabbit antibody (1:50) and peroxidase-conjugated rabbit

anti-goat antibody (1:50). For His48, secondary antibodies were peroxidase-conjugated rabbit anti-mouse antibody (1:50) and peroxidase-conjugated goat anti-rabbit antibody (1:50). These antibodies were applied in PBS containing 1% BSA and 5% normal rat serum. The sections were finally incubated with filtered AEC (10 mg/2.5 ml dimethylformamide in 50 ml 0.1 mol/l acetate buffer pH 5.0) containing 0.03% H_2O_2 for 10 min at room temperature. Counterstaining was performed with hematoxylin and the slides were covered with Kaiser's glycerin-gelatin. After each incubation, the sections were rinsed with PBS.

Enzyme histochemistry for detection of ROS formationAir-dried cryostat sections (4 μm) were stained with DAB to detect reactive oxygen species as described before with some modifications (26). Briefly, sections were washed in 0.1 N Tris-HCl buffer (pH 7.6) and subsequently incubated for 30 min at 60°C in 0.1 N Tris-HCl buffer containing 0.5 mg/ml DAB. ROS production and concomitant peroxidase activity induce the oxidation of DAB.

All liver cryostat sections were routinely stained with hematoxylin/eosin and periodic acid-Schiff to evaluate liver morphology.

Morphometric determinations

Up to 50 non-overlapping fields of methanol-fixed, paraffin-embedded samples were evaluated on at least two different sections for each animal in each treatment group. Morphometric determinations were performed using a computerized image analysis system connected to an Olympus microscope (Olympus Vanox AHBT3, Olympus Optical Co. Ltd., Tokyo, Japan).

Proliferating HSCs were defined (3, 5) as interstitial cells with at least one αSMA- positive cytoplasmic process extending along the sinusoidal wall of hepatocytes (thus excluding immunoreactive elements of the portal tracts) and a labeled nucleus.

The parenchymal extension of αSMA-positive cells was measured by point-counting technique. Data were expressed as a percentage of area (% of area=% of total parenchymal volume).

Western blotting

Livers were homogenized with a Polytron homogenizer in a buffer containing 20 mmol/l Tris-HCl (pH 7.2), 0.2 mmol/l phenylmethylsulfonylfluoride (PMSF), 1 mmol/l ethylenediaminetetraacetic acid (EDTA), and 1 mmol/l dithiothreitol. After centrifugation (30 min, 11 600×g), the protein concentration in the supernatant (crude lysate) was determined with the Bio-Rad protein assay (Bio-Rad Laboratories, Hercules, CA) using bovine serum albumin as standard. The crude lysates were fractionated on a 10% sodium dodecylsulfate polyacrylamide gel and transferred to nitrocellulose, using a semi-dry blotting system according to the manufacturer's instructions (Pharmacia, Uppsala, Sweden). Prestained molecular weight standards (Bio-Rad) were used as marker proteins. The blots were incubated with a 1:5000 dilution of the polyclonal iNOS antibody in PBS containing 4% skim milk powder and 0.1% Tween-20, subsequently incubated with horseradish peroxidase labeled swine anti-rabbit IgG and finally developed using the ECL Western blotting system (Amersham).

Analytical determinations

AST and ALT were determined by routine clinical chemistry. Nitrite+nitrate (NOx) concentrations in plasma and culture media were determined by the method of Moshage et al. (27).

Statistical analysis

Data are expressed as mean±SD. Group means were compared by ANOVA followed by the Student-Newman-Keuls test if the former was significant. A p value <0.05 was considered statistically significant.

In vitro results

Effect of NO donors and antioxidants on ROS formation

To test whether NO donors are able to scavenge ROS in HSCs cultures, the NO donor SNAP was added at various concentrations to cuvets containing 80 μmol/l cytochrome c in PBS. Generation of ROS was initiated by the addition of FeAsc and the change in absorbance at 550 nm, indicating the generation of ROS (20), was monitored in a spectrophotometer. In the absence of SNAP, a strong increase of absorbance was noted. SNAP dose-dependently reduced the absorbance change at 550 nm, indicating scavenging of ROS. The generation of ROS was also abolished when the ROS scavengers catalase (500 U/ml) and superoxide dismutase (300 U/ml) were added to medium. To verify that the effect was due to NO formation and ROS generating systems, another NO donor, S-nitrosoglutathione (SNOG), and another ROS generating system (xanthine oxidase/hypoxanthine) were also tested, yielding similar results as SNAP and 50 μmol/l Fe^{2+} per 100 μmol/l ascorbate, respectively (data not shown). Fig. 1 (panel A) depicts the results of the scavenging of ROS by NO donors and antioxidants.

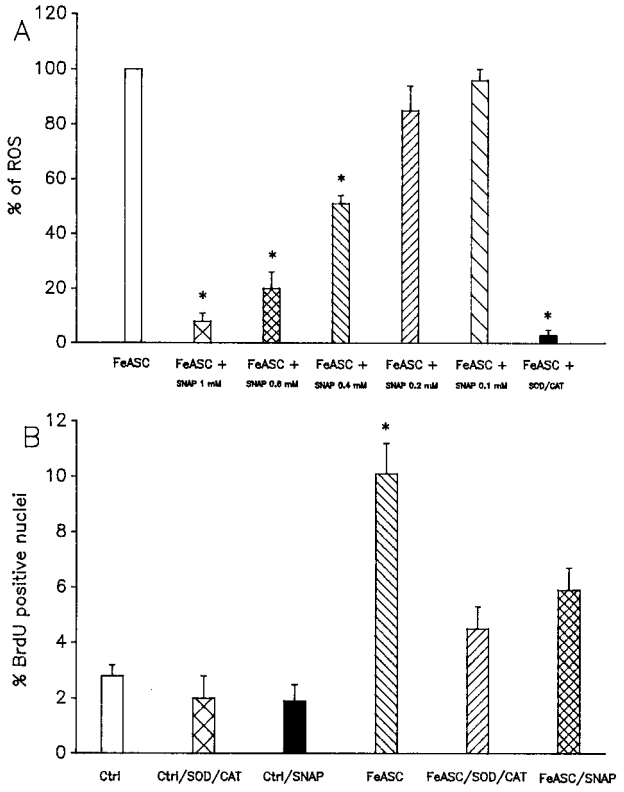

Fig. 1. Effect of NO donor and ROS scavengers on ROS production (panel A) and HSCs proliferation (panel B). Panel A: After incubation with FeAsc, ROS production was measured using the cytochrome c assay in HSCs in the presence of either different doses of SNAP or the ROS scavengers SOD (300 U/ml) and catalase (500 U/ml). Panel B: S-phase nuclei were identified by immunohistochemistry for BrdU in HSCs exposed to FeAsc in the presence or absence of either SNAP (1 mM) or the ROS scavengers SOD (300 U/ml) and catalase (500 U/ml). Data are presented as mean±SD. *$p<0.05$ vs controls.

Effect of ROS and NO donor on HSCs proliferation

To evaluate the effect of ROS and NO on HSCs proliferation, the nuclear incorporation of BrdU in S-phase cells was evaluated by immunohistochemistry (Fig. 1 panel B). The ROS donor FeAsc significantly increased BrdU incorporation in cultured HSCs, indicating enhanced cell proliferation. ROS-induced proliferation was abolished by the ROS scavengers catalase (500 U/ml) and superoxide dismutase (300 U/ml). In addition, the NO donor SNAP (1 mmol/l) also significantly reduced the ROS-induced HSCs proliferation. Neither the ROS scavengers nor the NO donor had any effect on basal proliferation of untreated HSCs.

Effect of FeAsc on 70 kD S6 kinase and ERK1/2 activation

It has been shown that intracellular signaling pathways involving either the phosphatidylinositol 3-kinase (PI3-K) or the extracellular-signal regulated kinase (ERK1/2) are stimulated by different cytokines and growth factors and regulate HSC proliferation and collagen synthesis (21–22). We thus performed Western blotting experiments to detect 70 kD S6 kinase and phosphorylated ERK1/2 in HSC extracts. The 70 kD S6 kinase is downstream from PI3-K and thus its activation is also an indirect measure of PI3-K activation (28, 29). Stimulation of 70 kD S6 kinase activity is paralleled by its increased phosphorylation on serine and threonine residues, resulting in a reduced mobility of the protein on sodium dodecyl sulfate-polyacrylamide gel electrophoresis (SDS-PAGE) (28–29). To evaluate ERK1/2 activation, ERK1/2 phosphorylation was determined by using antibody that specifically recognizes the active tyrosine-phosphorylated form of ERK-1 and ERK-2 (30). As shown in Fig. 2 (upper panel), PDGF (25 ng/ml, used as a positive control) (28) induce a decrease in the mobility of 70-kD and 85-kD triplets of proteins, as compared with controls, indicative of protein phosphorylation and enzyme activation. No effect on gel mobility was induced by FeAsc after either 10 or 30 min of incubation. Phosphorylated ERK1/2 (Fig. 2, lower panel) was barely detectable in control cells. FeAsc induced a striking increase in both ERK-1 and ERK-2 phosphorylation after 10 min of incubation that declined to control levels at 30 min. FeAsc-induced phosphorylation of both ERK-1 and ERK-2 at 10 min was inhibited down to control levels by HSC preincubation with 1 mmol/l SNAP.

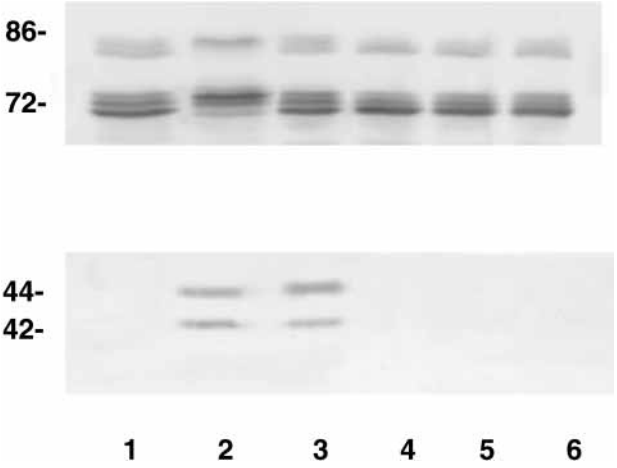

Fig. 2. Effect of FeAsc on 70 kD S6 kinase (upper panel) and ERK-1 and ERK-2 phosphorylation (lower panel). Cell lysates were obtained as described in Methods. Proteins (50 μg/lane) were separated by 9% SDS-PAGE, transferred to nitrocellulose and then incubated with specific antibodies. Lane 1: control. Lane 2: PDGF (25 ng/ml). Lane 3: FeAsc 10 min. Lane 4: FeAsc 10 min+SNAP. Lane 5: FeAsc 30 min. Lane 6: FeAsc 30 min+SNAP. Molecular-weight markers are represented on the left of each panel.

In vivo results

General effects of DMN treatment

Compared to controls (39.0±1.7 U/l), DMN treatment resulted in a striking increase in ALT values that was already evident 6 h after the third injection (286.5±21.3, $p<0.001$ vs controls) and peaked at 24 and 48 h (322.0±37.3 and 313.3±28.5, respectively, $p<0.001$). No differences in ALT value compared to controls were observed 1 week after the final DMN injection (50.1±4.7).

Six hours after the third DMN injection, evidence of hemorrhagic necrosis was observed in zone 3 associated with ballooning and lysis of hepatocytes, rare apoptotic bodies and infiltration of inflammatory cells. A massive perivenular hemorrhagic necrosis with a prominent inflammatory infiltrate was more evident at 24 h, associated with the appearance of centro-central bridging of necrotic areas (Fig. 3, panel A). The hemorrhagic necrosis of zone 3 was still observed at 48 h (Fig. 3, panel B), associated with lysis of the endothelium of the central vein, inflammatory infiltrate and persistence of thin centro-central bridging necrosis. At 1 week after the final DMN injection, liver sections showed only limited centro-central fibrotic septa (Fig. 3, panel C).

HSCs proliferation and activation

In controls (data not shown), αSMA-positive cells were detected mainly in the portal space either as elements of vascular walls or as fibroblast-like cells scattered in the connective tissue or finely apposed to bile ductules. In the lobule, immunoreactivity for αSMA was present in the walls of large- and medium-sized terminal hepatic veins.

To quantitate proliferating S-phase HSCs in the early phase of the process leading to liver fibrosis, we evaluated by morphometry the number of cells exhibiting one or more αSMA-positive cytoplasmic processes in conjunction with a PCNA positive nucleus (3, 5). Such cells were rarely observed in control rats. A significant increase of αSMA/PCNA positive cells was observed already at 6 h after the third DMN injection. These cells showed an elongated fibroblast-like shape and appeared particularly numerous in association with collapsed areas or groups of parenchymal cells in zone 3. Their number progressively increased throughout the experiments, reaching a maximum at 1 week after the final DMN injection (Fig. 4, panel A).

The amount of liver tissue occupied by αSMA-positive cells was evaluated by morphometry and expressed as the percentage of area. The area of liver parenchyma occupied by activated HSCs progressively increased, reaching a maximum at 1 week after the final DMN injection (Fig. 4, panel B). As shown in Fig. 5, these cells were initially observed close to the area of necrosis (panel A) and later accumulated to form αSMA-positive centro-central septa (panel B).

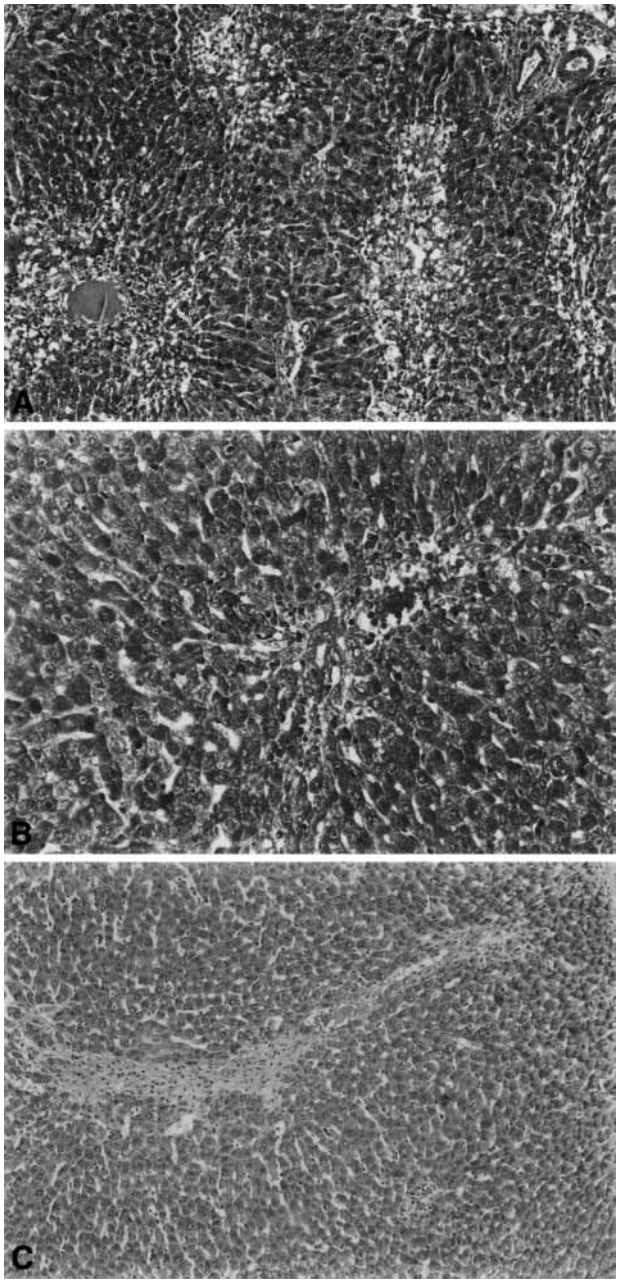

Fig. 3. Hematoxylin-eosin staining of liver sections at different time intervals after DMN administration. DMN (10 mg/kg) was administered for 3 consecutive days and sections were obtained at different time points. A massive perivenular hemorrhagic necrosis that spares the portal tract is evident in panel A (24 h, final magnification 25×). Necrotic areas are still observed at 48 h (panel B, final magnification 50×), while after 1 week (panel C, final magnification 25×) centro-central fibrotic septa are evident.

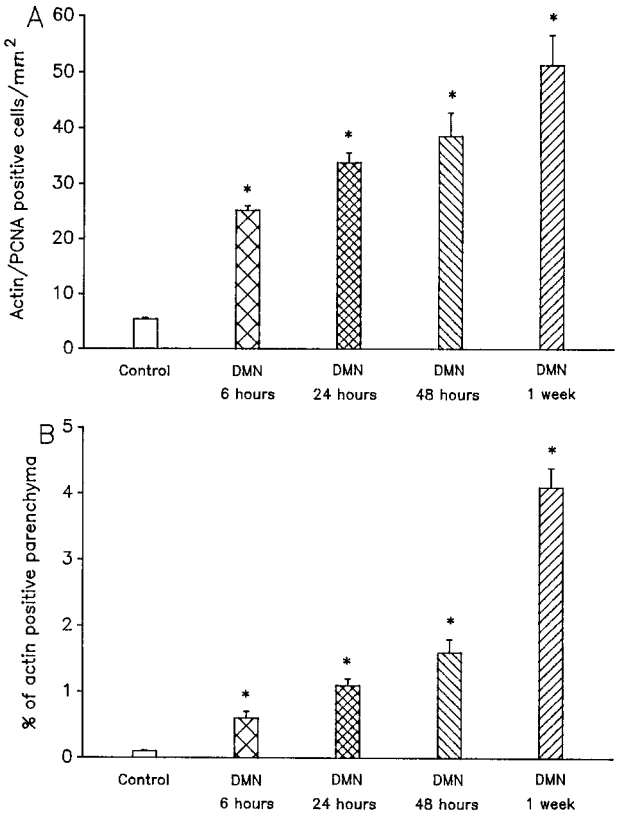

Fig. 4. Morphometric evaluation of HSCs proliferation and activation at different intervals after DMN treatment. Data were obtained by using a computerized image analysis system and expressed as number of cells/mm^2 for HSCs proliferation (panel A) and as a percent of liver parenchyma for HSCs activation (panel B). Data are expressed as mean±SD. *$p<0.05$ vs controls.

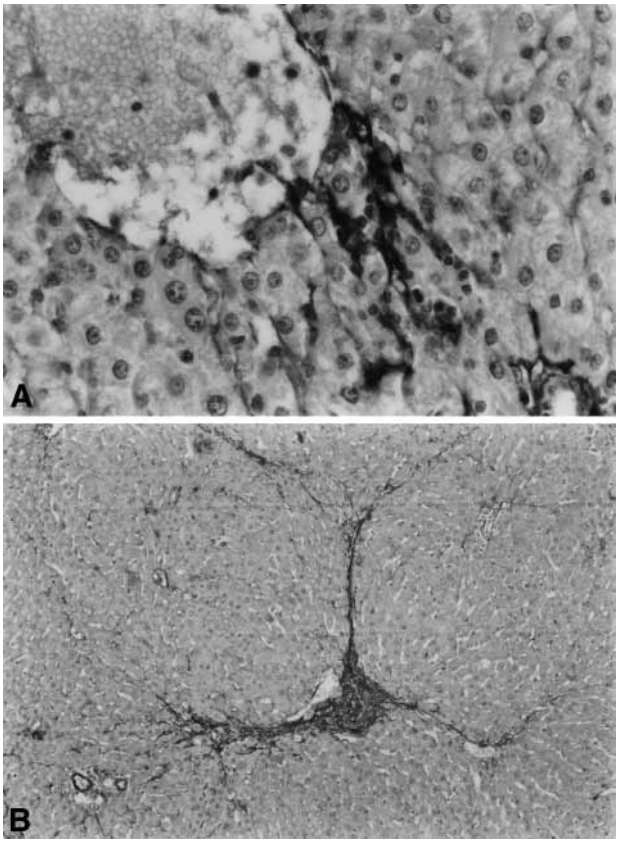

Fig. 5. Immunohistochemical staining for αSMA. αSMA-positive cells (i.e. activated HSCs) are initially observed in association with necrotic perivenular areas (panel A) and later accumulate, forming αSMA positive septa (panel B). Panel A: 48 h after DMN treatment (final magnification 100×). Panel B: 1 week after DMN treatment (final magnification 25×).

Localization of iNOS and neutrophils and ROS generation

In control liver, no iNOS staining was detectable, in accordance with previous studies (22). Six hours after the last DMN injection, a few scattered inflammatory cells expressed iNOS (Table 1). At later intervals, no iNOS staining was detectable. In accordance with immunohistological data, iNOS protein was not detectable by Western blot in liver homogenates, whereas iNOS protein was clearly expressed in liver tissue of endotoxin-treated rats (Fig. 6), used as positive control (24). The suitability of the antibody for immunohistochemistry has been demonstrated before (24). There was no increase of plasma NOx levels in DMN-treated rats compared to control animals (data not shown).

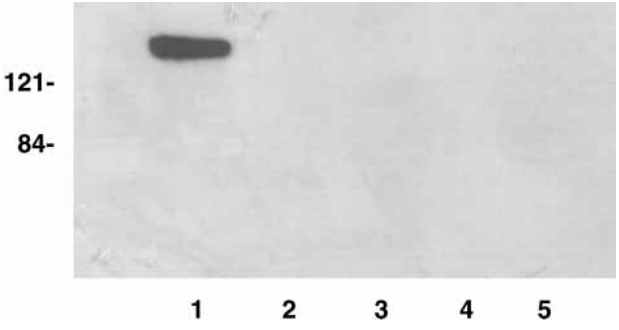

Fig. 6. iNOS protein level in LPS-treated rat liver (lane 1), normal rat liver (lane 2) and rat liver 6 h (lane 3), 24 h (lane 4), and 48 h (lane 5) after DMN treatment. Crude homogenates (50 μg/lane) were separated on a 10% SDS-PAGE gel, transferred to nitrocellulose and immunostained with antiserum against iNOS as described in Methods.

Neutrophil infiltration, as demonstrated by His48 staining, was strongly increased for at least 48 h after the last DMN injection (Fig. 7, panels A-C and Table 1), especially in areas of necrosis. Neutrophil numbers returned to near normal 1 week after the final DMN injection (Table 1). In control livers, only rare infiltrating neutrophils were present (Fig. 7, panel D). The enzyme histochemical demonstration of ROS generation (Fig. 8 and Table 1) showed a pattern of distribution iden-

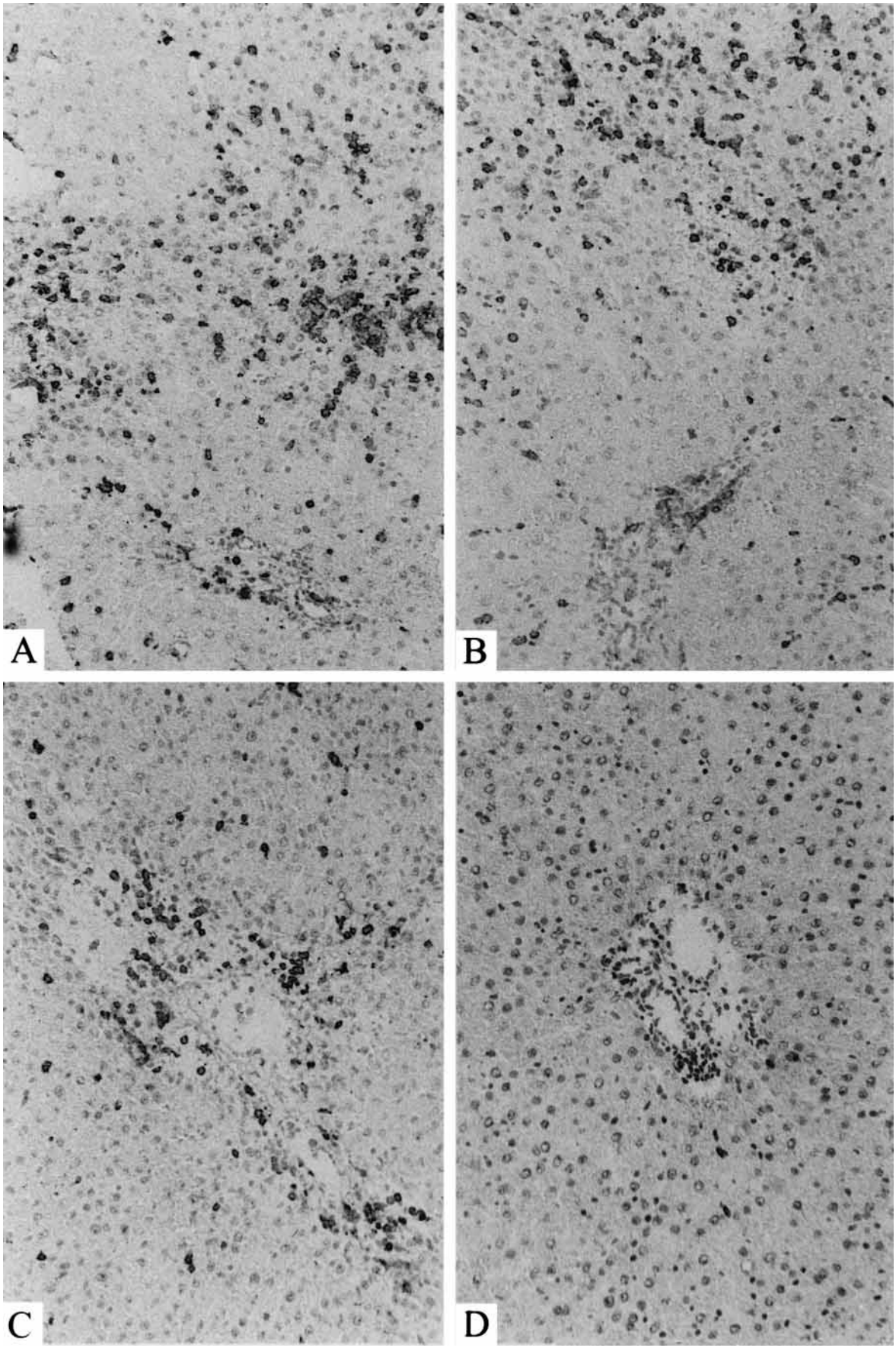
A
B
C
D

Table 1. iNOS expression, ROS generation and neutrophil infiltration at different time points after DMN treatment. + <10 positive cell/field; ++ 10–20 positive cell/field; +++ >20 positive cell/field

	6 h	24 h	48 h	7 days
iNOS	+	+/–	–	–
ROS	+++	++	++	+/–
Neutrophils	+++	++	++	+/–

tical to that of His48, suggesting that some of the infiltrating neutrophils are generating ROS.

Discussion

A common event in the initiation and progression of liver fibrosis is the activation of the hepatic stellate cell (HSCs) (1, 3, 5). Compared to quiescent HSCs, activated HSCs display increased expression of α-smooth muscle actin, synthesis of matrix components and proliferation (1). Triggers for activation are cytokines and reactive oxygen species (ROS). Indeed, it has been shown that ROS promote HSCs activation, matrix synthesis and proliferation *in vitro* (9–12). Circumstantial evidence is available which supports a similar role for ROS in the activation of HSCs *in vivo* (2, 6, 7). Therefore, any intervention aimed at reducing the exposure of HSCs to ROS could slow down or inhibit the progression of HSCs activation and fibrogenesis. Indeed, it has been demonstrated that the antioxidant vitamin E inhibits fibrogenesis in two different experimental models of liver fibrosis (6, 31).

The liver has ample resources to dispose of ROS, e.g. superoxide dismutases, catalase, glutathione, and vitamin E-like antioxidants. However, these ROS scavenging systems are mainly present in hepatocytes or compartmentalized in specific organelles like peroxisomes (catalase) and mitochondria (manganese superoxide dismutase) and will therefore not prevent HSCs from being exposed to ROS generated by infiltrating inflammatory cells. In this study we have demonstrated that infiltrating neutrophils are prominently present in the early phase of liver fibrosis. The neutrophilic infiltrate persisted for at least 48 h after the last DMN injection, but was significantly reduced 1 week after the last DMN injection. Neutrophils are

Fig. 7. Neutrophil identification by immunostaining for His48. Neutrophil infiltration was observed in areas of necrosis at 6 h (panel A), 24 h (panel B) and 48 h (panel C) after DMN treatment. Only rare neutrophils were observed at 1 week (data not shown) or in control livers (panel D). Final magnification 50×.

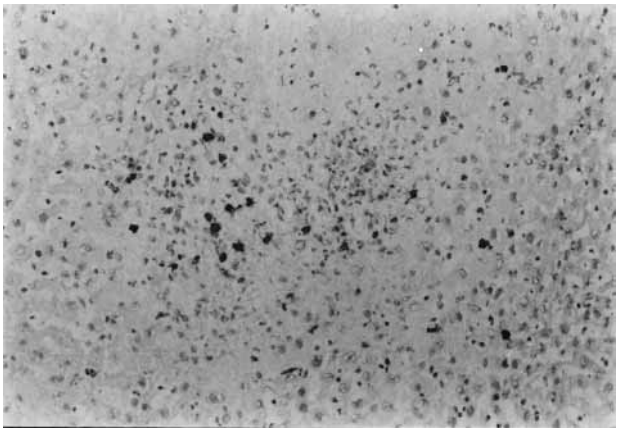

Fig. 8. ROS identification. ROS were identified by means of an enzyme histochemical reaction based on DAB oxidation. ROS formation was observed in area of necrosis with a spatial and temporal distribution similar to that of His48 positive cells, indicating that some of the neutrophils were producing ROS. Final magnification 25×.

known to be important producers of ROS (20). Indeed, as demonstrated in this study using an enzyme histochemical method to detect ROS generation, the infiltrating neutrophils produce significant amounts of ROS. ROS generation can be attributed to the infiltrating neutrophils, based on the similar spatiotemporal staining patterns for neutrophils and ROS generation. Interestingly, Casini et al. (32) have recently shown, using cocultures of peripheral blood neutrophils and HSCs, that neutrophils activated by *N*-formyl-Met-Leu-phenylalanine are potent producers of ROS and that neutrophil-derived ROS are able to stimulate matrix (i.e. type I collagen) synthesis in HSCs, supporting the notion that neutrophil-derived ROS are able to cause some aspects of HSCs activation. In agreement with this, *in vivo* data have shown a close relationship between neutrophil infiltration, generation of lipid peroxidation products and collagen deposition in another experimental model of liver fibrosis that benefits from neutrophil depletion (33, 34).

Nitric oxide (NO) radicals are able to react with ROS species like superoxide anions. The reaction of nitric oxide with superoxide anions yields peroxynitrite. Whether formation of peroxynitrite is beneficial or harmful is not clear and will most likely depend on the exact conditions of the microenvironment in which peroxynitrite is generated, such as the relative amounts of NO and superoxide anions, pH, and carbon dioxide concentration (17). On the one hand, peroxynitrite is a toxic and powerful oxidizing agent able to induce DNA damage, modify tyrosine residues in proteins into nitrotyrosine altering their shape and function, and induce lipid peroxidation (17, 35). On the

other hand, the reaction with nitric oxide removes superoxide anions, which are also highly reactive molecules able to induce lipid peroxidation (35). Casini et al. (32), using their *in vitro* coculture system of neutrophils and HSCs, demonstrated that inhibition of nitric oxide synthesis amplified the induction of collagen synthesis by neutrophil-derived ROS. Moreover, the ROS-induced collagen synthesis was partially inhibited by NO donors. In addition, several studies have demonstrated that inhibition of NO synthesis *in vivo* amplifies collagen synthesis in models of fibrosis in kidney and heart (36–37) and increases liver injury in both ethanol-treated rats (38) and in rats treated with sub-lethal doses of DMN (39). These studies support a ROS-scavenging beneficial role for NO in these models.

In the present study we have extended these findings to proliferation of HSCs, another prominent aspect of HSCs activation. Proliferation of HSCs was induced by a ROS-generating system (Fe/Asc) (9). We have also shown that HSCs incubation with FeAsc was associated with a striking increase in ERK1/2 activation, similar to that induced by PDGF used as a positive control. This is in agreement with previous papers which have indicated a key role of ERK activation in mediating fibroblasts and HSCs proliferation (21, 22, 40). Our data also confirm previous observations that have shown that moderate concentrations of ROS may act as intracellular messengers linking the effect of mitogenic cytokines to ERK activation (41, 42). In this cell type, Marra et al. (22) showed that ERK activation is at least partially PI3-K-dependent, because incubation with the PI3-K inhibitor wortmannin resulted in a 50% reduction in ERK activity. In this study, ERK activation following HSCs incubation with FeAsc is PI3-K-independent because no effects were observed on the activity of the 70 kD S6 kinase, which lies downstream of PI3-K (21, 28, 29).

ROS-induced proliferation of HSCs was inhibited by the ROS-scavengers superoxide dismutase/catalase and, most importantly, by the NO donor S-nitroso-N-acetylpenicillamine (SNAP), which also blocked FeAsc-induced ERK activation. Moreover, using the cytochrome c assay to monitor superoxide anion formation, we could demonstrate that SNAP-derived NO scavenges superoxide anions in a dose-dependent manner. Similar results were obtained when SNAP was substituted for another NO donor (S-nitroso-glutathione (SNOG)), and when Fe/Ascorbate was substituted for another ROS-generating system (xanthine oxidase/hypoxanthine) (data not shown), ruling out the possibility that the inhibitory effect of SNAP on superoxide anion formation and ROS-induced proliferation of HSCs was due to a peculiar effect of the combination of SNAP and Fe/Ascorbate.

To be an effective ROS-scavenger in inflammatory conditions *in vivo*, NO must be clearly produced at sites where ROS are generated. However, in the present model of liver injury, induction of iNOS was negligible. On Western blot, iNOS was not detectable in liver homogenates and, using immunohistochemistry, only a few iNOS-positive inflammatory cells were visible 6 h after the last DMN injection, but not at later time points after the last DMN injection. These observations demonstrate that in this model of liver injury no significant amount of NO is generated and that the ROS generated by infiltrating neutrophils are not scavenged by NO. It is tempting to speculate that the lack of NO synthesis is, at least partially, responsible for the progression of HSCs activation and fibrogenesis. To test this possibility it will be necessary to apply NO generating systems in experimental models of fibrosis, for instance using iNOS-expressing adenoviruses, as recently described by Billiar and coworkers (43, 44). These iNOS-expressing adenoviruses have already been used in a model of intimal hyperplasia and in a model of apoptotic liver injury, yielding impressive beneficial results. The notion that the lack of NO synthesis favors the progression of fibrosis is supported by studies using models of fibrosis in other organs, in particular heart and kidney. In these models, as stated above, inhibition of NO synthesis has profound stimulatory effects on the synthesis of matrix proteins like collagen and on the progression of fibrosis (36, 37). In addition, we have recently shown that iNOS is weakly and transiently induced in the bile duct ligation model of liver fibrosis (45). Inhibition of NO synthesis in this model results in increased deposition of collagen around necrotic areas, although this effect is very transient and is not reflected by an increase in total liver hydroxyproline content (manuscript submitted).

In summary, we have shown that NO can prevent ROS-induced HSCs proliferation, a prominent aspect of HSCs activation, by virtue of its capacity to scavenge superoxide anions. HSCs activation in DMN-induced liver injury is likely to be mediated by increased ROS generation, since abundant infiltration with ROS-generating neutrophils in this model was demonstrated. However, this mechanism of NO-mediated ROS-scavenging is probably not significant *in vivo*, since iNOS and consequently NO production are hardly induced in this experimental models of liver fibrosis. Interventions aimed at increasing hepatic expression of iNOS and/or NO generation could reduce HSCs activation and fibrogenesis.

Acknowledgments

Part of this work was presented at the annual meeting of the American Association for the Study of Liver Diseases, Chicago, Illinois, November 9, 1997 and at the annual meeting of the European Association for the Study of the Liver, Lisbon, Portugal, 1998.

The authors wish to thank Prof. A.M. Jezequel (Department of Experimental Pathology, University of Ancona) for the helpful discussion. The expert technical assistance of A. de Jager-Krikken is gratefully acknowledged.

This work was supported by grants from MURST 1998.

References

1. Olaso E, Friedman S L. Molecular regulation of hepatic fibrogenesis. J Hepatol 1998; 29: 836–47.
2. Tsukamoto H, Matsuoka M, French S W. Experimental models of hepatic fibrosis: a review. Semin Liv Dis 1990; 10: 56–65.
3. Mancini R, Jezequel A M, Benedetti A, et al. Quantitative analysis of proliferating sinusoidal cells in dimethylnitrosamine-induced cirrhosis. An immunohistochemical study. J Hepatol 1992; 15: 361–6.
4. Geerts A, Lazou J M, De Bleser P, Wisse E. Tissue distribution, quantitation and proliferation kinetics of fat-storing cells in carbon tetrachloride-injured rat liver. Hepatology 1991; 13: 1193–202.
5. Svegliati-Baroni G, D'Ambrosio L, Curto P, et al. Interferon gamma decreases hepatic stellate cells activation and extracellular matrix deposition in rat liver fibrosis. Hepatology 1996; 23: 1189–99.
6. Pietrangelo A, et al. Molecular and cellular aspects of iron-induced hepatic cirrhosis in rodents. J Clin Invest 1995; 95: 1824–31.
7. Pietrangelo A. Metals, oxidative stress and hepatic fibrogenesis. Semin Liver Dis 1996; 16: 13–30.
8. Ahotupa M, Bereziat J C, Bussachini-Griot V, et al. Lipid peroxidation induced by n-nitrosodimethylamine (NDMA) in rats *in vivo* and in isolated hepatocytes. Free Rad Res Commun 1987; 3: 285–91.
9. Lee K S, Buck M, Chojkier M. Activation of hepatic stellate cells by TGFα and collagen type I is mediated by oxidative stress through c-myb expression. J Clin Invest 1995; 96: 2461–8.
10. Svegliati-Baroni G, D'Ambrosio L, Ferretti G, et al. Fibrogenic effect of oxidative stress on rat hepatic stellate cells. Hepatology 1998; 27: 720–6.
11. Svegliati-Baroni G, Di Sario A, Casini A, et al. The Na^+/H^+ exchanger modulates the fibrogenic effect of oxidative stress in rat hepatic stellate cell. J Hepatol 1999; 30: 868–75.
12. Parola M, Pinzani M, Casini A, et al. Stimulation of lipid peroxidation or 4-hydroxynonenal treatment increases procollagen α1(I) gene expression in human liver fat-storing cells. Biochem Biophys Res Commun 1993; 194: 1044–50.
13. Parola M, Leonarduzzi G, Robino G, et al. On the role of lipid peroxidation in the pathogenesis of liver damage induced by long-standing cholestasis. Free Rad Biol Med 1996; 20: 351–9.
14. Michel T, Feron O. Nitric oxide synthases: Which, where, how and why? J Clin Invest 1997; 100: 2146–52.
15. Förstermann U, Kleinert H. Nitric oxide synthase: expression and expressional control of the three isoforms. Naunyn-Schmiedeberg's Arch Pharmacol 1995; 352: 351–64.
16. Moncada S, Palmer R M J, Higgs E A. Nitric oxide: physiology, pathophysiology and pharmacology. Pharmacol Rev 1991; 43: 109–42.
17. Beckman J S, Koppenol W H. Nitric oxide, superoxide, and peroxynitrite: the good, the bad, and the ugly. Am J Physiol 1996; 271: C1424–37.
18. Billiar T R. The delicate balance of nitric oxide and superoxide in liver pathology. Gastroenterology 1995; 108: 603–5.
19. Di Sario A, Svegliati-Baroni G, Bendia E, et al. Characterization of ion transport mechanisms regulating intracellular pH in hepatic stellate cells. Am J Physiol 1997; 273: G39–48.
20. O'Brien P J. Superoxide production. Meth Enzymol 1984; 105: 370–8.
21. Svegliati-Baroni G, Ridolfi F, Di Sario A, et al. Insulin and insulin-like growth factor-1 stimulate proliferation and type I collagen accumulation by human hepatic stellate cells: differential effects on signal transduction pathways. Hepatology 1999; 29: 1743–51.
22. Marra F, Pinzani M, De Franco R, et al. Involvement of phosphatidylinositol 3-kinase in the activation of extracellular signal-regulated kinase by PDGF in hepatic stellate cells. FEBS Lett 1995; 376: 141–5.
23. Mancini R, Marucci L, Benedetti A, et al. Immunohistochemical analysis of S-phase cells in normal human and rat liver by PC10 monoclonal antibody. Liver 1994; 14: 57–64.
24. Vos T A, Gouw A S H, Klok P A, et al. Differential effects of nitric oxide synthase inhibitors on endotoxin-induced liver damage in rats. Gastroenterology 1997; 113: 1323–33.
25. van Goor H, Fidler V, Weening J J, Grond J. Determinants of focal and segmental glomerulosclerosis in the rat after renal ablation. Evidence for involvement of macrophages and lipids. Lab Invest 1991; 64: 754–65.
26. Poelstra K, Hardonk M J, Koudstaal J, Bakker W W. Intraglomerular platelet aggregation and experimental glomerulonephritis. Kidney Int 1990; 37: 1500–8.
27. Moshage H, Kok B, Huizenga J R, Jansen P L M. Nitrite and nitrate determinations in plasma: a critical evaluation. Clin Chem 1995; 41: 892–6.
28. Chung J, Grammer T C, Lemon K P, et al. PDGF- and insulin-dependent $pp70^{S6K}$ activation mediated by phosphatidylinositol-3-OH kinase. Nature 1994; 370: 71–5.
29. Cheatham B, Vlahos C J, Cheatham L, et al. Phosphatidylinositol 3-kinase activation is required for insulin stimulation of pp70 S6 kinase, DNA synthesis and glucose transporter translocation. Mol Cel Biol 1994; 14: 4902–11.
30. Yung Y, Dolginov Y, Yao Z, et al. Detection of ERK activation by a novel monoclonal antibody. FEBS Lett 1997; 408: 292–6.
31. Parola M, Leonarduzzi G, Biasi F, et al. Vitamin E dietary supplementation protects against carbontetrachloride-induced chronic liver damage and cirrhosis. Hepatology 1992; 16: 1014–21.
32. Casini A, Ceni E, Salzano R, et al. Neutrophil-derived superoxide anion induces lipid peroxidation and stimulates collagen synthesis in human hepatic stellate cells: role of nitric oxide. Hepatology 1997; 25: 361–7.
33. Parola M, Leonarduzzi G, Robino G, et al. On the role of lipid peroxidation in the pathogenesis of liver damage induced by long-standing cholestasis. Free Rad Biol Med 1996; 20: 351–9.
34. Saito J M, Maher J J. Bile duct ligation in rats induces biliary expression of cytokine-induced neutrophil chemoattractant. Gastroenterology 2000; 118: 1157–68.
35. Darley-Usmar V, Wiseman H, Halliwell B. Nitric oxide and oxygen radicals: a question of balance. FEBS Lett 1995; 369: 131–5.
36. Chatziantoniou C, Boffa J-J, Ardaillou R, Dussaul J-C. Nitric oxide inhibition induces early activation of type I collagen gene in renal resistance vessels and glomeruli in transgenic mice. J Clin Invest 1998; 101: 2780–9.

37. Hou J, Kato H, Cohen R A, et al. Angiotensin II-induced cardiac fibrosis in the rat is increased by chronic inhibition of nitric oxide synthase. J Clin Invest 1995; 96: 2469–77.
38. Nanji A A, Greenberg S S, Tahan S R, et al. Nitric oxide production in experimental alcoholic liver disease in the rat: role in protection from injury. Gastroenterology 1995; 109: 899–907.
39. Nagase S, Isobe H, Ayukawa K, et al. Inhibition of nitric oxide production increases dimethylnitrosamine-induced liver injury in rats. J Hepatol 1995; 23: 601–4.
40. Pages G, Lenormand P, L'Allemain G, et al. Mitogen-activated protein kinases $p42^{mapk}$ and $p44^{mapk}$ are required for fibroblast proliferation. Proc Natl Acad Sci USA 1993; 90: 8319–23.
41. Sundaresan M, Yu Z X, Ferrans V J, et al. Requirement for generation of H_2O_2 for platelet-derived growth factor signal transduction. Science 1995; 270: 296–9.
42. Gonzalez-Rubia M, Voit S, Rodriguez-Puyol D, et al. Oxidative stress induces tyrosine phosphorylation of PDGF alpha- and beta-receptors and pp60c-src in mesangial cells. Kidney Int 1996; 50: 164–73.
43. Tzeng E, Billiar T R, Williams D L, et al. Adenovirus-mediated inducible nitric oxide synthase gene transfer inhibits hepatocyte apoptosis. Surgery 1998; 124: 278–83.
44. Shears L L, Kibbe M R, Murdock A D, et al. Efficient inhibition of intimal hyperplasia by adenovirus-mediated inducible nitric oxide synthase gene transfer to rats and pigs *in vivo*. J Am Coll Surg 1998; 187: 295–306.
45. Beljaars E, Vos T A, Poelstra K, et al. Expression of iNOS during the development of liver fibrosis in rats. Cells Hepatic Sinusoid 1997; 6: 32–3.